Regional earthquake as a trigger for enhanced volcanic activity: Evidence from MODIS thermal data

Andrew J. L. Harris[1] and Maurizio Ripepe[2]

Received 25 September 2006; revised 29 November 2006; accepted 7 December 2006; published 25 January 2007.

[1] The magnitude 6.4 earthquake that occurred in Java on 26 May 2006 provided us with data capable of revealing an immediate eruptive response at two Javanese volcanoes, Merapi and Semeru. The availability of pre-processed thermal data for volcanic hot spots detected by the Moderate Resolution Imaging Spectrometer (MODIS), and provided on http://hotspot.higp.hawaii.edu, allowed us to produce heat and volume flux time series for these two erupting volcanoes covering a 35-day period spanning the earthquake. Our results revealed a coupled response by the volcanoes to the earthquake, both experiencing increases in heat and volume flux beginning 3 days after the earthquake, with the response lasting 9 days. The response was felt at both volcanoes as a factor of two-to-three increase in the rate of volumetric output, after which output returned to the pre-response rates. This implies that the earthquake triggered enhanced output at two erupting volcanoes 50 and 300 km distant from the earthquake epicenter and separated from each other by ~260 km. **Citation:** Harris, A. J. L., and M. Ripepe (2007), Regional earthquake as a trigger for enhanced volcanic activity: Evidence from MODIS thermal data, *Geophys. Res. Lett.*, *34*, L02304, doi:10.1029/2006GL028251.

1. Introduction

[2] Determining the factors that drive changes in volcanic activity are of primary importance in understanding how and why a volcano erupts. Such insights aid in monitoring and forecasting volcanic activity. By changing the stress field around a volcano regional tectonic events can force changes in volcanic activity; triggering volcano seismicity [*West et al.*, 2005], intrusive and effusive events [*Walter and Amelung*, 2006] or, possibly, an explosive eruption [*Linde and Sacks*, 1998]. As a result, there has long been debate as to how large regional earthquakes can trigger eruptions [*Hill et al.*, 2002]. The November 1975 Kilauea (Hawaii), the 1991 Pinatubo (Philippines), and the 1960 Cordon Caulle (Chile) eruptions, for example, have all been linked with large regional earthquakes [*Tilling et al.*, 1976; *Bautista et al.*, 1996; *Lara et al.*, 2004]. The lag between the Pinatubo eruption and a magnitude 7.8 earthquake ~100 km to the NE was, however, 11 months. Also, many other significant earthquakes have occurred without triggering new eruptions at nearby volcanoes, e.g. the 26 December 2004 Sumatra-Andaman earthquake. To link regional earthquake and volcanic activity, an eruption at one or more well monitored volcanoes must be underway during a regional tectonic event.

[3] The magnitude 6.4 earthquake that occurred 455 km ESE of Jakarta (Figure 1) on 26 May 2006 (22:53:58 UTC) provided us with an opportunity to examine the eruptive responses at two Javanese volcanoes. Initially the earthquake, striking early in the local morning (05:53:58 am, 27 May 2006, local time), with an epicenter depth of ~10 km, caused significant damage and fatalities [*Nakano et al.*, 2006]. At the time of the earthquake two Javanese volcanoes were active: Merapi and Semeru. The two volcanoes are ~260 km apart and were ~50 km north and ~280 km east of the earthquake epicenter, respectively (Figure 1). Each were also being checked for thermal anomalies using satellite sensors as part of routine global hot spot monitoring run by Hawaii Institute of Geophysics and Planetology. The resulting data base allowed us to search for any heat and volumetric responses at Merapi and Semeru over a 35-day-long period (10 May to 14 June) spanning the earthquake.

2. MODIS-Derived Radiance Data for Merapi and Semeru

[4] To obtain radiance data for the two volcanoes we used output from the Moderate Resolution Imaging Spectroradiometer (MODIS) volcanic hot spot detection algorithm, (MODVOLC) as given on http://hotspot.higp.hawaii.edu [*Wright et al.*, 2002]. MODVOLC is a non-interactive algorithm that uses low spatial resolution (1-km pixel) satellite data acquired by the National Atmospheric and Space Administration (NASA) MODIS sensor to detect and map global thermal anomalies. MODVOLC scans the MODIS data stream searching for evidence of sub-pixel hot spots. Once a hot spot is identified, its details (time, location, emitted spectral radiance, satellite observation geometry) are written to ASCII text files and disseminated via global hot spot maps [*Wright et al.*, 2004]. These data can be used to determine the presence, radiant intensity and heat flux of volcano-related hot spots [e.g., *Wright and Flynn*, 2004].

[5] MODIS sensors are flown on NASA's Terra and Aqua satellites. These two polar orbiting satellites have return periods of ~12 hours, so that any point on the earth's surface can, if cloud-free, be imaged twice a day by each satellite, for a total of four images/day using both satellites. Overpass times for Terra are ~15:00 and ~03:00, and for Aqua ~06:00 and ~18:00 (all times are UT). During 10 May to 14 June, 2006, hot spots were detected by MODVOLC at Merapi during 36 Terra and Aqua over-

[1] Hawaii Institute of Geophysics and Planetology, School of Oceanography and Earth Science Technology, University of Hawaii, Honolulu, USA.
[2] Dipartimento di Scienze della Terra, Università di Firenze, Florence, Italy.

0094-8276/07/2006GL028251$05.00

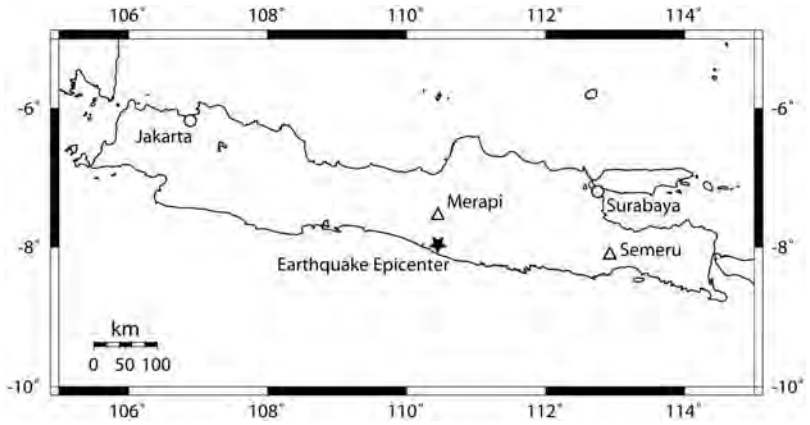

Figure 1. Island of Java with location of Merapi (7.54°S, 110.44°E) and Semeru (8.11°S, 112.92°E) volcanoes (triangles), major cities (circles), and the epicenter of the 26 May 2006 earthquake (star) at 7.89°S, 110.41°E [*Nakano et al.*, 2006].

passes, and at Semeru during 20 overpasses. Given a total of 140 overpasses by Terra and Aqua during this 35-day-long period, this means that cloud cover prevented hot spot detection for 74 and 86% of the overpasses at Merapi and Semeru, respectively.

[6] At Merapi the number of thermally anomalous pixels detected during an overpass remained stable (Figure 2a). The maximum band 21 radiance ($B21_{max}$) for detected pixels, however, increased from a mean ($\pm 1\sigma$) of 1.1 ± 0.6 W/m^2 sr μm before the earthquake to 2.6 ± 1.6 W/m^2 sr μm after it (Figure 2b). The band 21 radiance summed for all detected pixels during an overpass (ΣB21) showed an identical trend, with the mean increasing from 1.7 ± 1.4 to 3.7 ± 2.4 W/m^2 sr μm (Figure 2c). Similarly, at Semeru, the number of thermally anomalous pixels remained stable (Figure 2d). Semeru's $B21_{max}$, however, doubled from a mean of 0.9 ± 0.3 W/m^2 sr μm before the earthquake to 1.9 ± 1.3 W/m^2 sr μm after it (Figure 2e); with ΣB21 increasing from 1.0 ± 0.4 to 2.5 ± 1.3 W/m^2 sr μm (Figure 2f).

[7] Sub-pixel cloud or plume contamination will reduce spectral radiances, and observations will be effected by viewing geometry effects, where pixel sizes increase with off-nadir viewing and hot spot shadowing will occur for features within deep craters [e.g., *Harris et al.*, 1997a, 1997b]. This will introduce noise into the time series and may mean that single point peaks and troughs cannot be trusted. However, consistent long term trends, confirmed by similar radiances recorded across multiple data points can reveal changes in activity [e.g., *Harris et al.*, 1997a; *Wright et al.*, 2002]. Radiances will also be contaminated by solar-reflection by day and require atmospheric correction [e.g., *Oppenheimer et al.*, 1993; *Harris and Stevenson*, 1997]; this is achieved using a MODTRAN modeled atmosphere.

3. Heat and Volume Fluxes for Merapi and Semeru

[8] We use the MODVOLC radiance data to estimate the heat and volume flux at the two volcanoes by applying the methodologies developed by *Harris et al.* [1997a, 1997b]. This was initially developed and tested using data for active basaltic lava flows [e.g., *Harris et al.*, 1998], but was adapted and tested for application to lava domes and silicic lava flows by *Harris et al.* [2003]. The method involves the following steps and assumptions.

[9] First, lava area is calculated by assuming that a hot spot pixel contains a hot (lava) source at temperature T_h surrounded by a cooler (ambient) background at T_b. Together these two sources contribute to the pixel integrated temperature (T_{int}) so that:

$$L(T_{int}, \lambda) = p\,L(T_h, \lambda) + (1 - p)\,L(T_b, \lambda) \quad (1)$$

in which L is the Planck function for a blackbody radiating at temperature T and wavelength λ, and p is the pixel portion occupied by the hot source [*Oppenheimer et al.*, 1993]. Following *Wright and Flynn* [2004] we obtain T_{int} from MODIS band 21 (3.939 μm) pixel-integrated radiances given in the MODVOLC text files; this waveband being highly sensitive to sub-pixel hot spots. The background temperature is obtained from band 32 (12.02 μm) pixel-integrated radiances. This waveband is less sensitive to sub-pixel hot spots, thus the signal is assumed to be dominated by the ambient background [*Wright and Flynn*, 2004].

[10] Following *Harris et al.* [1997a, 1997b], to estimate the pixel portion occupied by the hot volcanic source we assumed a range of likely hot spot surface temperatures (T_h). These we set as follows. We assume a two component thermal structure for the dome surface comprising an extensive cooled carapace at T_{crust} broken by cracks that expose the hot dome interior at T_{core} and occupy fraction f of the surface. We set T_{core} to the maximum expected temperature at Merapi of ~1000°C [*Voight and Davies*, 2000]. Then, following satellite-based thermal analyses of Lascar, Unzen and Santiaguito lava domes [*Oppenheimer et al.*, 1993; *Wooster et al.*, 2000; *Harris et al.*, 2003], we set f to ~0.005 and T_{crust} to 150–250°C. This gives an effective radiation temperature, $T_e = [f T_{core}^4 + (1 - f) T_{crust}^4]^{0.25}$ [*Crisp and Baloga*, 1990], of 150–270°C. We use this range to describe the typical surface temperatures for the entire dome unit, and thus the likely sub-pixel hot spot temperature. Broadening this range will widen our envelope of solutions for p, and all following parameter-calculations based in this initial estimate for p, but will not change the trends.

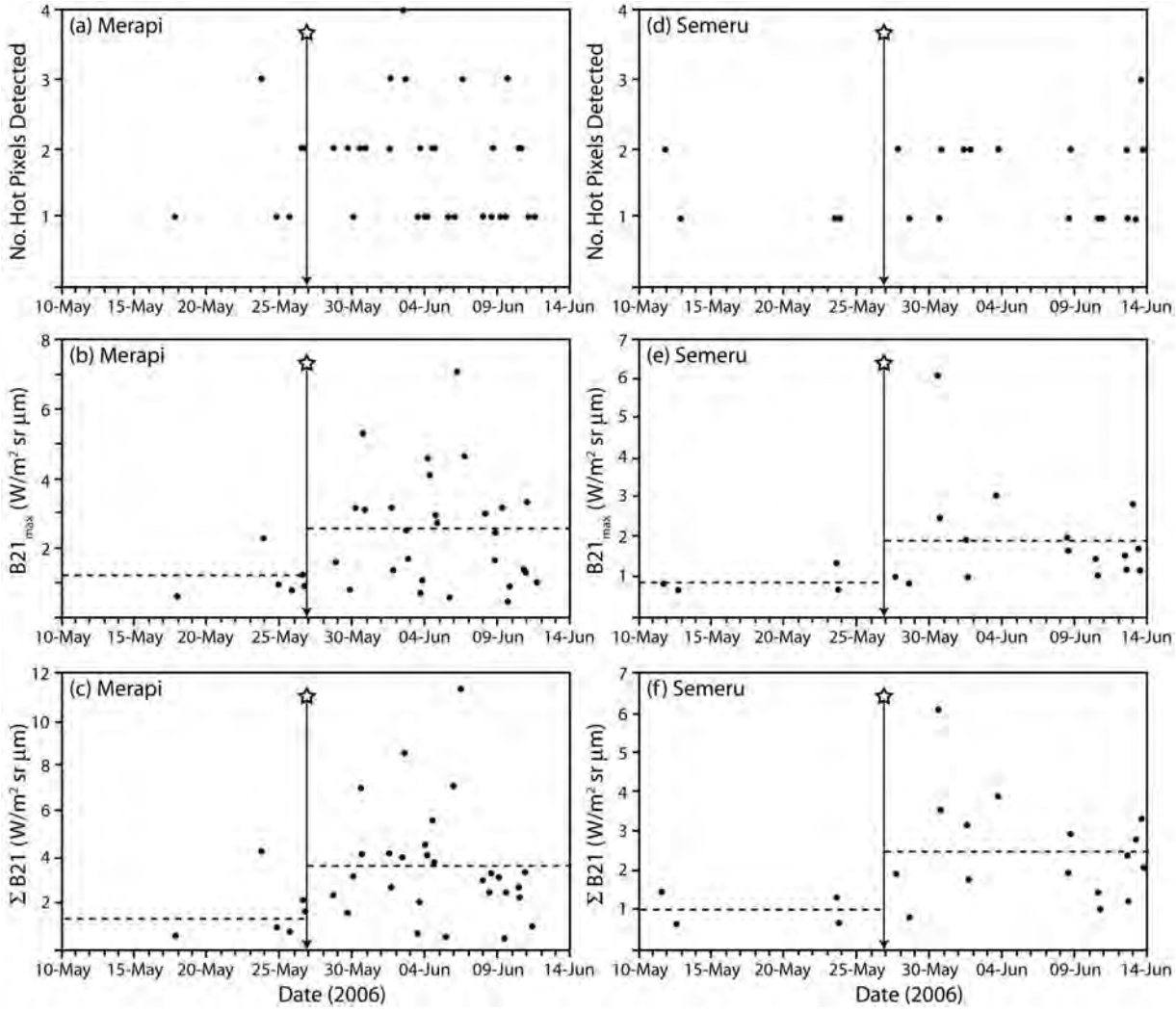

Figure 2. Number of thermally anomalous pixels detected by MODVOLC, maximum band 21 radiance ($B21_{max}$) for detected pixels and sum of all band 21 pixel radiances (ΣB21) detected during each overpass for (a–c) Merapi and (d–f) Semeru during 10 May to 14 June, 2006. Dashed horizontal lines indicate mean levels before and after the earthquake, and the star linked to the arrow marks the temporal position of the 26 May earthquake.

[11] Multiplying p by pixel area (1 km^2) and then summing for all located pixels on a particular image gives total lava area (A) at the time of image acquisition. Given lava area, radiative [$Q_{rad} = A\sigma\varepsilon T_h^4$] and convective [$Q_{conv} = h_c\,(T_h - T_{air})$] heat fluxes can now be calculated. Here, σ, ε, h_c and T_{air} are the Stefan-Boltzmann constant (5.67×10^{-8} W m^{-2} K^{-4}), emissivity of Andesite (0.98 [*Salisbury and D'Aria*, 1992, 1994]) convective heat transfer coefficient for an active lava (~50 W m^{-2} K^{-1}) and ambient air temperature (25°C), respectively. For our lava temperature range this gives two end member heat flux cases, a cold (T_h = 150°C) and hot (T_h = 270°C) case, respectively (Figure 3).

[12] Estimated heat fluxes are then used to calculate the volume flux (E) from:

$$E = Q_{tot}/\rho\left(c_p\Delta T + L\varphi\right) \quad (2)$$

in which Q_{tot} is total heat loss (= Q_{rad} + Q_{conv}), L is latent heat of crystallization (3.5×10^5 J/kg K) and φ is post eruption crystallization. We note that our calculation of Q_{tot} assumes surface heat losses dominate the thermal budget, and that heat loss by basal conduction from a dome overlying an active conduit is insignificant. Microtextural analyses of the Merapi lava domes emplaced between 1986 and 1995 give crystal volume fractions of up to ~0.75, of which 0.25–0.45 are due to microlite growth [*Hammer et al.*, 2000]. We therefore use a maximum post eruption crystallization of 0.45. Lava density (ρ = 2600 kg/m^3) and specific heat capacity (c_p = 1150 J/kg K) are corrected for vesicularities of 10–30 %. Because components of the 22 November 1994 block and ash flow deposits derived from the 1992–1994 dome complex were dominantly represented by "poorly vesicular, crystalline lithics" [*Abdurachman et al.*, 2000], we favor a low vesicularity. Finally, post extrusion cooling (ΔT) of the unit interior by 200–350°C is used [*Harris et al.*, 2003]. This gives a range of volume fluxes for each MODVOLC volcanic hot spot detection (Figure 3). Given that all but Q_{tot} are assumed, this conversion assumes a linear relationship between heat and

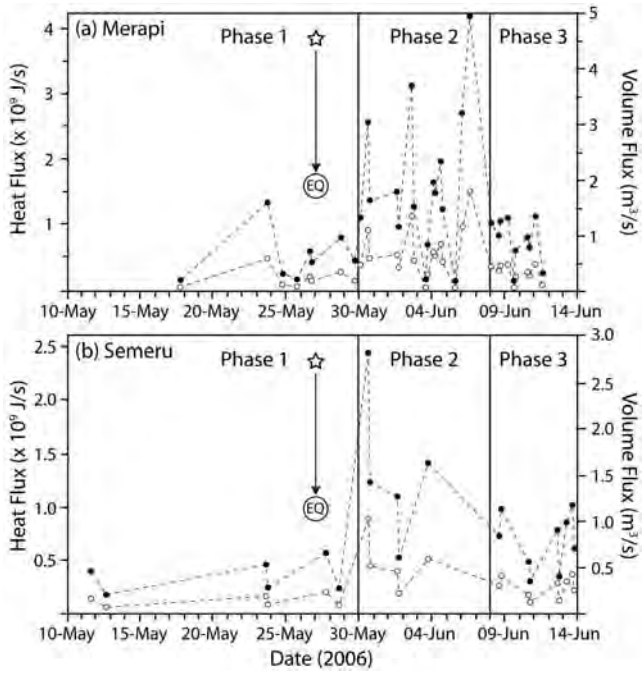

Figure 3. Heat and volume flux ranges calculated using MODVOLC data for (a) Merapi and (b) Semeru during 10 May to 14 June. The temporal position of the 26 May earthquake is marked with a star linked to the "EQ" label. The three heat and volume flux defined eruption phases are marked. In each case maximum (filled circle) and minimum (open circle) bounds are placed on the heat or volume flux through application of cold (T_h = 150°C, ΔT = 200°C, vesicularity 10%) and hot (T_h = 270°C, ΔT = 350°C, vesicularity 30%) models.

volume flux [*Wright et al.*, 2001]; we hence plot Q_{tot} on the left hand axis and the equivalent E on the right axis of Figure 3.

[13] As pointed out by *Wright et al.* [2001], because of the assumptions involved in applying equation (2), the main variable becomes lava area (all other parameters are assumed and constant), so that volume flux becomes directly related to lava area. For the two cases given here we can thus reduce equation (2) to $E = 10.925A$, for the cold model, and $E = 20.949A$, for the hot model, A being active lava area in km^2. Given that active lava area is, itself, based on the summed band 21 radiance and an assumed (set and constant) range of lava temperatures, this can be reduced further allowing E to be obtained directed from ΣB_{21}. Given our assumed values for lava temperature, crystallization and cooling, we obtain $E = 0.450\Sigma B_{21} - 0.127$, for the cold model, and $E = 0.164\Sigma B_{21} - 0.045$, for the hot model.

4. Merapi and Semeru Heat and Volume Fluxes, May–June 2006

[14] Between 17 May and 14 June, we obtain heat fluxes for Merapi in the range 0.6 to 42.2 $\times$ 10^8 J/s. These convert to volume fluxes in the range 0.1 to 4.9 m^3/s, with a mean of 0.9 m^3/s. Three phases of activity could be identified on the basis of heat and volume flux (Figure 3a). The first phase spanned 17–29 May and was characterized by relatively low heat fluxes, typically 3.7 ± 3.4 $\times$ 10^8 J/s. The second phase began on 30 May and was characterized by higher fluxes, 11.2 ± 9.6 $\times$ 10^8 J/s with peaks at 20–40 $\times$ 10^8 J/s. The final phase was underway by 8 June and was marked by a return to lower fluxes of 5.3 ± 3.7 $\times$ 10^8 J/s; similar to those of the first phase. In terms of volume flux, this converts to an increase from 0.4 ± 0.4 m^3/s during the first phase to 1.3 ± 1.1 m^3/s by phase 2, before falling back to 0.6 ± 0.4 m^3/s during phase 3 (Figure 3a). The phase 2 mean of 1.3 m^3/s compares with a ground based estimate of 1.1 m^3/s on 8 June (Monthly reports: Merapi, Smithsonian Institution Bulletin of the Global Volcanism Network, available at http://www.volcano.si.edu/).

[15] By integrating the heat flux through time we obtain total power for the 28 day period spanning 17 May–14 June of 1.7 ± 0.9 $\times$ 10^{15} J. This converts to a total extruded volume for this period of 2 ± 1 $\times$ 10^6 m^3. This compares with a ground-based dome volume of ~2.3 $\times$ 10^6 m^3 emplaced between the onset of extrusion (~10 April) and 22 May (Monthly reports: Merapi, Smithsonian Institution

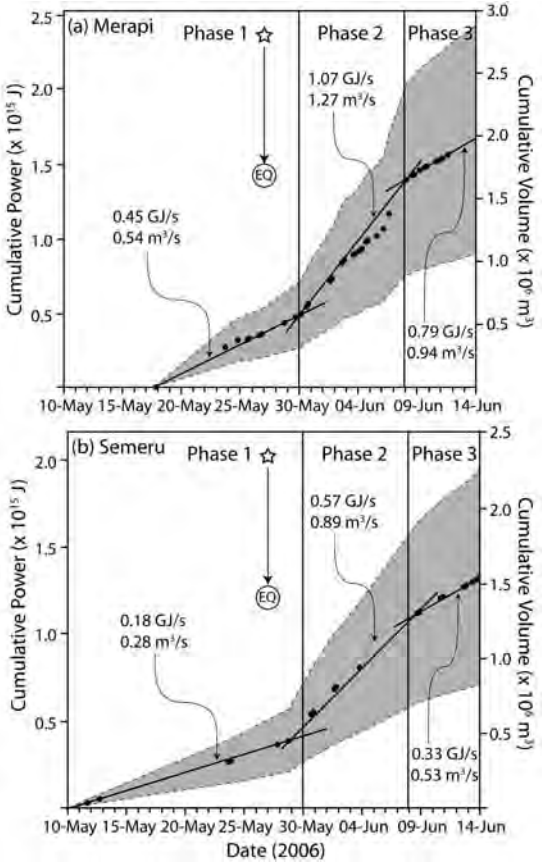

Figure 4. Envelope of cumulative power and volume (gray zone) for (a) Merapi and (b) Semeru from integration heat and volume fluxes given in Figure 3. The mid-point for each measurement (filled circle) and linear best fit through mid-point-values is given for each phase. The position of the earthquake and three eruption phases are marked as in Figure 3.

Bulletin of the Global Volcanism Network, available at http://www.volcano.si.edu/). The cumulative power and volume plots reveal the same three phases from inflections in the rate of increase of the total power and lava volume, with a high heat and volume flux phase beginning ~3 days after the 26 May earthquake and lasting ~9 days (Figure 4a).

[16] At Semeru, for the period 10 May to 14 June 2006, we obtain heat fluxes in the range 0.6 to 24.1 $\times$ 10^8 J/s. These convert to volume fluxes of 0.1 to 2.8 m^3/s, with a mean of 0.8 m^3/s. As at Merapi, three phases of activity can be identified on the basis of heat and volume flux (Figure 3b). The first phase was characterized by relatively low fluxes, typically 2.4 $\pm$ 1.6 $\times$ 10^8 J/s and 0.3 $\pm$ 0.2 m^3/s, and ended between 28 and 30 May. The second phase began with a peak in the heat and volume flux on 30 May and had typical fluxes of 8.9 $\pm$ 6.7 $\times$ 10^8 J/s and 1.1 $\pm$ 0.8 m^3/s. By 8 June heat and volume fluxes had returned to lower values (4.6 $\pm$ 2.9 $\times$ 10^8 J/s and 0.6 $\pm$ 0.3 m^3/s); a level more typical of that obtained during the first phase. For Semeru, we obtain a total power over the 35 day period spanning 10 May to 14 June of 1.3 $\pm$ 0.6 $\times$ 10^{15} J, which converts to a total extruded volume of 1.5 $\pm$ 0.7 $\times$ 10^6 m^3. As at Merapi, the cumulative power and volume revealed an increase around 30 May (Figure 4b). This increase lasted ~9 days until 8 June; at which point fluxes returned to levels similar of those prior to 30 May.

[17] Heat and volume flux trends over the 35-day-period spanning the earthquake were almost identical at Merapi and Semeru, where we identify a ~9-day-long high heat and volume flux phase, beginning ~3 days after the 26 May earthquake at both volcanoes. During this phase calculated heat and volume fluxes increased by a factor of 2.4 and 3.2 at the two volcanoes, respectively. The increases at Merapi are consistent with field-based observations which report an increase in activity following the 26 May earthquake, with lava dome volumes and flow lengths approximately doubling (Monthly reports: Merapi, Smithsonian Institution Bulletin of the Global Volcanism Network, available at http://www.volcano.si.edu/). In addition, gas plumes reached 1300 m above the summit on 1 June, compared with 500 m on 25 May, and multiple pyroclastic flows extended up to ~4 km during 31 May to 6 June (Monthly reports: Merapi, Smithsonian Institution Bulletin of the Global Volcanism Network, available at http://www.volcano. si.edu/).

[18] The increase in the sub-pixel hot spot area, and hence heat flux, may have been due not only to increases in the area and temperature of the dome and associated lava flows, but also to hot material emplaced by pyroclastic flows. This would still indicate increased activity, but influenced by increased in pyroclastic rather than extrusive activity. However, three factors lead us to believe that the band 21 radiance was dominated by a hot lava source at the volcano summit. First, the anomaly pixel size that we consider is constant (Figures 2a and 2d), with a location centered on the summits of both volcanoes with no flank anomalies. Second, most of the increase in summed radiance results from an increase in intensity of the 3.959 μm signal (Figures 2b and 2e); suggesting an increase in area of a hot, lava-like, sub-pixel source. Third, the increase in calculated volume flux matches that indicated by ground reports given in Bulletin of the Global Volcanism Network (available at http://www.volcano.si.edu/).

5. Relationship With the 26 May Earthquake

[19] We thus find simultaneous and identical trends in heat and volume flux at both volcanoes during 10 May to 14 June (Figures 2–4). Given that the two volcanoes are separated by 260 km, we conclude that the coupled behavior was a response to changes in the static and/or dynamic stresses forced by the 26 May earthquake. Static stresses are defined by *Hill et al.* [2002] as the "difference in the stress field from just before an earthquake to shortly after the seismic waves have decayed" and the dynamic stresses as those induced "by the seismic waves from a large earthquake."

[20] Because static stresses decay as $1/r^3$, r being the distance from the earthquake epicenter, their effects are limited to distances ranging from a few fault lengths to a maximum of a few 100 km [*Hill et al.*, 2002]. In our case, changes in static stress could be invoked to alter the pressure incident on a deeper chamber; increased compression causing magma to be squeezed upwards [*Hill et al.*, 2002]. An increase in the pressure difference along an open conduit between the source and the surface may be expected to force an increase in the rate of volumetric output [e.g., *Wadge*, 1981; *Dvorak and Dzurisin*, 1993; *Rowland et al.*, 2003]. However, given the distance of Semeru from the earthquake epicenter, an explanation involving dynamic stresses may be more appropriate.

[21] Dynamic stresses decay less rapidly with distance from earthquake epicenter ($1/r^{1.66}$) and can thus influence activity at more distant volcanoes [*Manga and Brodsky*, 2006], where passage of seismic waves can cause bubble diffusion [*Brodsky et al.*, 1998]. Such a mechanism could act as a vesiculation pump to cause enhanced eruption rates. *West et al.* [2005] invoked a fluid pump model to explain a local earthquake swarm at Mount Wrangell (Alaska, USA) ~1 hour following the 26 December 2004 Sumatra-Andaman earthquake 11,000 km away from Wrangell. In this model, pressure increases squeeze magma from interconnected pore space into nearby fault zones [*Brodsky and Prejean*, 2005]. In the case of Wrangell, the system was closed (not erupting) and no new eruption was triggered. Instead a local earthquake swarm was initiated and reflected a response characterized by shear failure possibly followed by fluid pumping into the fault zone [*West et al.*, 2005]. In our cases, the systems at Merapi and Semeru were open (erupting) so that magma may have been pumped into the open conduit system connecting the deeper source to the erupting vent, to be felt at the vent as a spurt in the erupted volume flux.

[22] The responses at Merapi and Semeru lagged ~72 hours behind the trigger (regional seismic) event. This may reflect the time it took the change felt by magma residing at deeper levels to be transmitted to the surface. Existence of a shallow magma chamber 1.5–2.5 km below the summit has been proposed at Merapi on the basis of seismic data [*Ratdomopurdo and Poupinet*, 2000]. Given such a depth the pulse would have been transmitted upwards at a rate of 500–800 m/day, to be felt at the surface 3 days after the trigger event. The effect, however, was

short-lived, with the volume fluxes returning to values typical of those prior to the earthquake after ~9 days, indicating that the effect (changes in the static and/or dynamic stresses) and symptom (increase in erupted volume flux) was transient and short-lived.

6. Conclusions

[23] Previous work has focused on attempting to draw links between regional seismic events and eruption onset [e.g., *Linde and Sacks*, 1998] thereby answering the question: *can a major regional earthquake trigger a volcanic eruption?* However, as at Mount Wrangell following the Sumatra-Andaman earthquake [*West et al.*, 2005], no new eruptions were triggered by the 26 May Java earthquake. Instead, those two eruptions that were under-way within Java experienced coupled responses in terms of their eruptive intensity, measured in terms of heat and erupted volume flux. We conclude that regional earthquake events are not always able to trigger an eruption itself, but do have sufficient influence to modify the intensity of activity at on-going eruptions. In the cases documented by us, the response was immediate but relatively short-lived, with pre-earthquake conditions being returned to within 12 days of the triggering earthquake. Regional earthquakes can thus effect on-going volcanic eruptions, but in our case the influence only extended over the time scale of a few days. Hence, studies that attempt to link earthquakes solely to new volcanic eruptions and/or activity over longer time-frames will miss any correlated activity responses at erupting or persistently active volcanoes. Instead, eruption parameters at volcanoes active during regional earthquakes must be carefully and continuously measured in the days immediately before, during and after an earthquake if a link is to be found.

[24] **Acknowledgments.** This work was prompted and initially supported by the Department of Civil Protection of the Italian Ministry of the Interior through the DEVnet project of the University of Firenze. AJLH was funded by NASA grant NMG04G064G "New Tools for Advanced Hot-Spot Tracking using MODIS Thermal Alerts." We are grateful to Julia Hammer for discussions regarding the likely post-eruption crystallization of Merapi's lava, Andrea Steffke for locating and ordering all MODIS Level 1b data and cloud products, and to two anonymous reviews whose insightful suggestions greatly improved this manuscript.

References

Abdurachman, E. K., J.-L. Bourdier, and B. Voight (2000), Nuées ardentes of 22 November 1994 at Merapi volcano, Java, Indonesia, *J. Volcanol. Geotherm. Res.*, *100*, 345–361.

Bautista, B. C., L. P. Bautista, R. S. Stein, E. S. Barcelona, R. S. Punongbayan, E. P. Laguerta, A. R. Rasdas, G. Ambubuyog, and A. Q. Amin (1996), Relationship of regional and local structures to Mount Pinatubo activity, in *Fire and Mud*, edited by C. G. Newhall and R. S. Punongbayan, pp. 351–370, Univ. of Wash. Press, Seattle.

Brodsky, E. E., and S. G. Prejean (2005), New constraints on mechanisms of remotely triggered seismicity at Long Valley Caldera, *J. Geophys. Res.*, *110*, B04302, doi:10.1029/2004JB003211.

Brodsky, E. E., B. Sturtevant, and H. Kanamori (1998), Earthquakes, volcanoes, and rectified diffusion, *J. Geophys. Res.*, *103*, 23,827–23,838.

Crisp, J., and S. Baloga (1990), A model for lava flows with two thermal components, *J. Geophys. Res.*, *95*, 1255–1270.

Dvorak, J. J., and D. Dzurisin (1993), Variations in magma supply rate at Kilauea Volcano, Hawaii, *J. Geophys. Res.*, *98*, 22,255–22,268.

Hammer, J. E., K. V. Cashman, and B. Voight (2000), Magmatic processes revealed by textural and composition trends in Merapi dome lavas, *J. Volcanol. Geotherm. Res.*, *100*, 165–192.

Harris, A. J. L., and D. S. Stevenson (1997), Thermal observations of degassing open conduits and fumaroles at Stromboli and Vulcano using remotely sensed data, *J. Volcanol. Geotherm. Res.*, *76*, 175–198.

Harris, A. J. L., S. Blake, D. A. Rothery, and N. F. Stevens (1997a), A chronology of the 1991 to 1993 Etna eruption using AVHRR data: Implications for real time thermal volcano monitoring, *J. Geophys. Res.*, *102*, 7985–8003.

Harris, A. J. L., A. L. Butterworth, R. W. Carlton, I. Downey, P. Miller, P. Navarro, and D. A. Rothery (1997b), Low cost volcano surveillance from space: Case studies from Etna, Krafla, Cerro Negro, Fogo, Lascar, and Erebus, *Bull. Volcanol.*, *59*, 49–64.

Harris, A. J. L., L. P. Flynn, L. Keszthelyi, P. J. Mouginis-Mark, S. K. Rowland, and J. A. Resing (1998), Calculation of lava effusion rates from Landsat TM data, *Bull. Volcanol.*, *60*, 52–71.

Harris, A. J. L., L. P. Flynn, and W. I. Rose (2003), Temporal trends in lava dome extrusion at Santiaguito 1922–2000, *Bull. Volcanol.*, *65*, 77–89.

Hill, D. P., F. Pollitz, and C. Newhall (2002), Earthquake-volcano interactions, *Phys. Today*, *55*(11), 41–47.

Lara, L. E., J. A. Naranjo, and H. Moreno (2004), Rhyodacitic fissure eruption in southern Andes (Cordon Caulle; 40.5 degrees S) after the 1960 (Mw: 9.5) Chilean earthquake: A structural interpretation, *J. Volcanol. Geotherm. Res.*, *138*, 127–138.

Linde, A. T., and I. S. Sacks (1998), Triggering of volcanic eruptions, *Nature*, *395*, 888–890.

Manga, M., and E. Brodsky (2006), Seismic triggering of eruptions in the far field: Volcanoes and geysers, *Annu. Rev. Earth Planet. Sci.*, *34*, 263–291.

Nakano, M., H. Kumagai, K. Miyakawa, T. Yamashina, H. Inoue, M. Ishida, A. Aoi, N. Morikawa, and P. Harjadi (2006), Source estimates of the May 2006 Java earthquake, *EOS Trans. AGU*, *87*(45), 493.

Oppenheimer, C., P. W. Francis, D. A. Rothery, R. W. Carlton, and L. S. Glaze (1993), Infrared image analysis of volcanic thermal features: Lascar volcano, Chile, 1984–1992, *J. Geophys. Res.*, *98*, 4269–4286.

Ratdomopurdo, A., and G. Poupinet (2000), An overview of the seismicity of Merapi volcano (Java, Indonesia), 1983–1994, *J. Volcanol. Geotherm. Res.*, *100*, 193–214.

Rowland, S. K., A. J. L. Harris, M. J. Wooster, F. Amelung, H. Garbeil, L. Wilson, and P. J. Mouginis-Mark (2003), Volumetric characteristics of lava flows from interferometric radar and multispectral satellite data, *Bull. Volcanol.*, *65*, 311–330.

Salisbury, J. W., and D. M. D'Aria (1992), Emissivity of terrestrial materials in the 8–14 μm atmospheric window, *Remote Sens. Environ.*, *42*, 83–106.

Salisbury, J. W., and D. M. D'Aria (1994), Emissivity of terrestrial materials in the 3–5 μm atmospheric window, *Remote Sens. Environ.*, *47*, 345–361.

Tilling, R. I., R. Y. Koyanagi, P. W. Lipman, J. P. Lockwood, J. G. Moore, and D. A. Swanson (1976), Earthquake and related catastrophic events, Island of Hawaii, November 29, 1975: A preliminary report, *U. S. Geol. Surv. Circ.*, *740*, 33 pp.

Voight, B., and M. J. Davies (2000), Emplacement temperatures of the November 22, 1994 nuée ardente deposits, Merapi volcano, Java, *J. Volcanol. Geotherm. Res.*, *100*, 371–377.

Wadge, G. (1981), The variation of magma discharge rate during basaltic eruptions, *J. Volcanol. Geotherm. Res.*, *11*, 139–168.

Walter, T. R., and F. Amelung (2006), Volcano-earthquake interaction at Mauna Loa volcano, Hawaii, *J. Geophys. Res.*, *111*, B05204, doi:10.1029/2005JB003861.

West, J., J. J. Sánchez, and S. R. McNutt (2005), Periodically triggered seismicity at Mount Wrangell, Alaska, after the Sumatra earthquake, *Science*, *308*, 1144–1146.

Wooster, M. J., T. Kaneko, S. Nakada, and H. Shimizu (2000), Discrimination of lava dome activity styles using satellite-derived thermal structures, *J. Volcanol. Geotherm. Res.*, *102*, 97–118.

Wright, R., and L. Flynn (2004), Space-based estimate of the volcanic heat flux into the atmosphere during 2001 and 2002, *Geology*, *32*(3), 189–192.

Wright, R., S. Blake, A. Harris, and D. Rothery (2001), A simple explanation for the space-based calculation of lava eruptions rates, *Earth Planet. Sci. Lett.*, *192*, 223–233.

Wright, R., L. Flynn, H. Garbeil, A. Harris, and E. Pilger (2002), Automated volcanic eruption detection using MODIS, *Remote Sens. Environ.*, *82*, 135–155.

Wright, R., L. P. Flynn, H. Garbeil, A. J. L. Harris, and E. Pilger (2004), MODVOLC: Near-real-time thermal monitoring of global volcanism, *J. Volcanol. Geotherm. Res.*, *135*, 29–49.

A. J. L. Harris, Hawaii Institute of Geophysics and Planetology, School of Oceanography and Earth Science Technology, University of Hawaii, 1680 East-West Road, Honolulu, HI 96822, USA. (harris@higp.hawaii.edu)

M. Ripepe, Dipartimento di Scienze della Terra, Università di Firenze, via G. La Pira, 4, 50121, Firenze, Italy.